Progress In Electromagnetics Research Letters, Vol. 90, 7–13, 2020

Eight-Element with H-Shaped Slot MIMO Antenna for 5G Applications

Zhong Yu, Yuqing Chen*, Yongbin Xie, and Nan Guo

Abstract—An eight-element multiple-input-multiple-output antenna system which consists of H-shaped slot antennas is presented around the handset frame for 5G applications. Each antenna element consists of an H-shaped radiating surface and an L-shaped microstrip feeder. In the frequency bands of 3.4–3.6 GHz and 4.7–5.1 GHz, the isolation is lower than −15 dB by introducing the ladder-shaped defect ground structure. The antenna efficiency is 50%–81%, and the envelope correlation coefficient is lower than 0.02 among antenna elements. The measurement results agree well with the simulation ones, indicating that the proposed antenna can satisfy the requirements of 5G communication.

1. INTRODUCTION

Recently, multiple-input-multiple-output (MIMO) technology in 5G handsets has been widely used for high data rates and throughput scenarios [1–5]. Besides, it has become a trend to design multiple antennas in a compact space of handset. However, how to reduce the mutual coupling between the adjacent antennas especially eight-element MIMO antennas in one handset is a critical problem.

In [6], an single-frequency MIMO antenna is proposed, which consists of six monopole elements and four slot elements arranged alternately. The isolation between adjacent antennas is only −11 dB without any decoupling structure. Liu et al. propose a dual-band eight-element PIFA antenna with bandwidth of 170 MHz at a center frequency of 2.6 GHz and bandwidth of 300 MHz at a center frequency of 5 GHz [7]. The vertical metal patch increases the isolation to −12.5 dB on the corner of the terminal and −10 dB on the edge. In [8], a four-band eight-element MIMO antenna is presented. Four monopole antennas of different shapes, F, C, L, and S, are used as the radiation surface of each antenna element. The protruding structure of inverted-π is used as a decoupling element to increase the isolation to −20 dB. Each antenna element occupies a space of $15 \times 25 \times 1.6\,\text{mm}^3$ on the side of the terminal, which is not suitable to integrate in a handset. Li et al. design a high-isolation eight-element MIMO antenna with balanced open slots as antenna elements [9]. The isolation between antenna elements is higher than −17.5 dB, and the efficiency is greater than 62% by reducing the ground effect. However, this antenna only covers a single operating frequency band of 3.4–3.6 GHz. Compared with the various types of antennas proposed above, slot antennas [10, 11] can be easily integrated into an compact terminals with high efficiency and high performance.

In this letter, an eight-element multiple-input-multiple-output antenna system which consists of H-shaped slot antennas operating in 3.4–3.6 GHz and 4.7–5.1 GHz for 5G handsets is presented. This antenna system is designed around the frame of the handset to save space and reduce isolation. The rectangular open end is added into H-shaped main radiating surface to cover the dual bands. Moreover, the isolation among adjacent antennas can be effectively reduced by adjusting the length and width of the defective ground structure (DGS). This letter measures the antenna characteristic and performance, including S-parameters, radiation patterns, antenna efficiencies, and the envelope correlation coefficients (ECC).

Received 7 November 2019, Accepted 22 January 2020, Scheduled 3 February 2020
* Corresponding author: Yuqing Chen (cyq940471251@163.com).
The authors are with the School of Xi'an University of Posts & Telecommunications, Xi'an, China.

2. ANTENNA DESIGN AND ANALYSIS

The proposed eight-element multiple-input-multiple-output antenna system which consists of H-shaped slot antennas is symmetrically designed on an FR4 substrate ($\varepsilon_r = 4.4$ and $\delta = 0.02$) with thickness of 1 mm, as shown in Figure 1(a). The dimension of the handset system is $140 \times 70 \times 1\,\text{mm}^3$ which is a typical dimension for a 5-inch handset. Each antenna element occupies a small space of $18.3 \times 2.5\,\text{mm}^2$ and the H-shaped slot as the main radiation surface of the antenna element. Figure 1(b) shows the dimensions of each slot antenna element, and the detailed values of the parameters are given in Table 1.

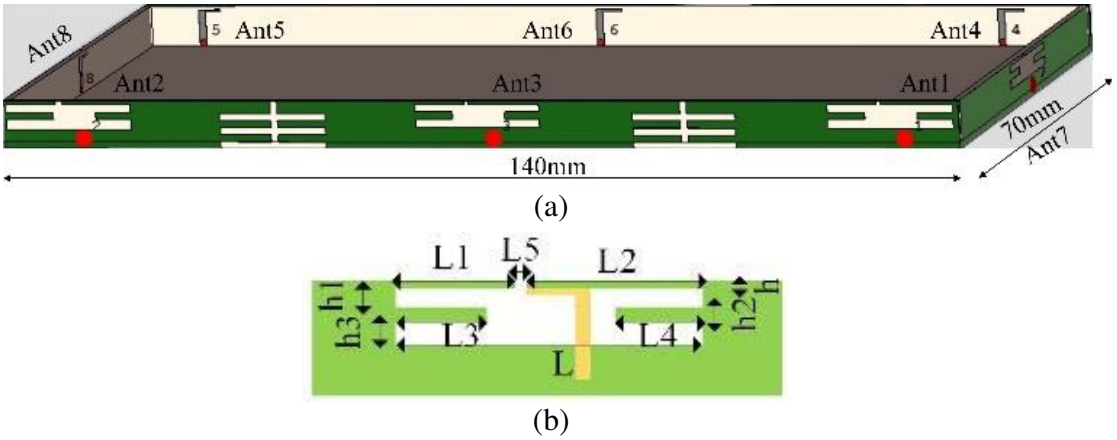

Figure 1. Geometry of the MIMO antennas: (a) overall view; and (a) detailed dimensions of antenna element.

Table 1. Parameters of each slot antenna.

Name	Ant1	Ant2	Ant3	Ant4	Ant5	Ant6	Ant7	Ant8
L/mm	18.24	18.20	17.90	18.15	18.10	17.57	18.05	18.20
$L1$/mm	7.10	7.50	7.10	7.80	6.80	6.87	7.20	7.30
$L2$/mm	10.50	10.40	10.20	10.35	10.70	10.10	10.05	10.10
$L3$/mm	5.44	6.10	5.30	5.56	6.40	5.07	5.50	5.60
$L4$/mm	5.20	5.50	4.90	5.35	5.80	4.80	4.95	5.00
$L5$/mm	0.65	1.00	0.60	1.00	1.00	0.60	0.80	0.80
h/mm	0.50	0.50	0.50	0.50	0.50	0.50	0.50	0.50
$h1$/mm	1.00	1.10	1.00	1.00	1.10	1.10	0.80	0.80
$h2$/mm	1.00	1.00	1.00	1.00	1.00	1.00	1.00	1.00
$h3$/mm	1.30	1.50	1.30	1.60	1.50	1.40	1.20	1.20

Compared with the rectangular slot, the H-shaped slot reduces the width of the slot radiator and increases the size of the ground, which makes it easier to achieve high isolation and efficiency of the antenna. The rectangular open end of $0.5 \times 0.5\,\text{mm}^2$ divides the radiation surface into two parts, which is added in the upper portion of the H-shaped slot. The right part of $L2, L4, h$, and $h2$ generates the low-order mode to cover the 3.4–3.6 GHz band, while the left part of $L1, L3, h1$, and $h3$ generates the high-order mode to fully cover the 4.7–5.1 GHz band.

Figure 2 shows the surface current distribution of each antenna element at the resonant frequency, and the arrow is the current flow direction. The L-shaped microstrip line printed on the front surface of the substrate is used for coupling and feeding, which forms a microstrip line-gap coupling feeding structure. The lengths in the horizontal and vertical directions are 5.3 mm and 4 mm, respectively. The antenna matching can be optimized by adjusting the port positions.

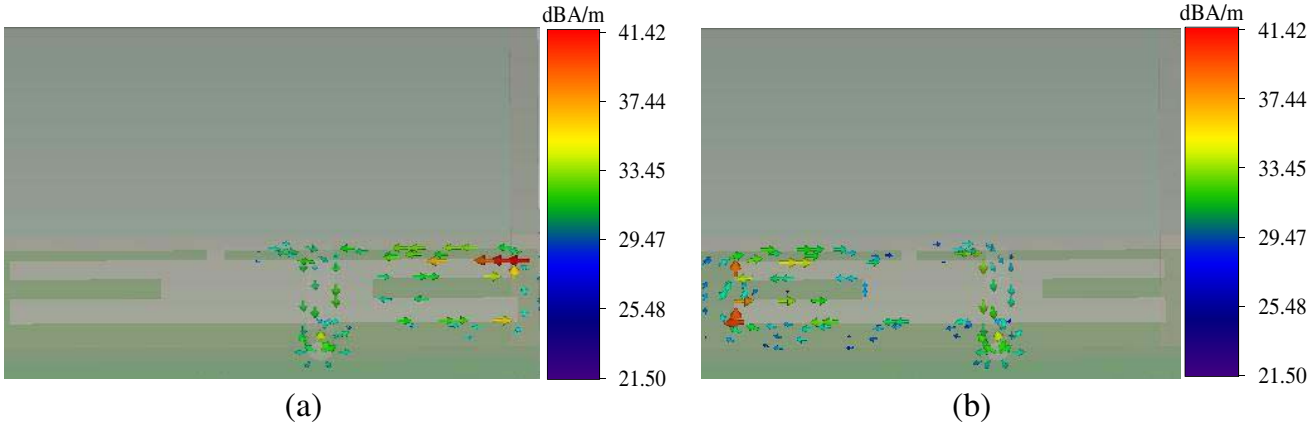

Figure 2. Current distribution on the antenna surface: (a) at 3.5 GHz; and (b) at 4.9 GHz.

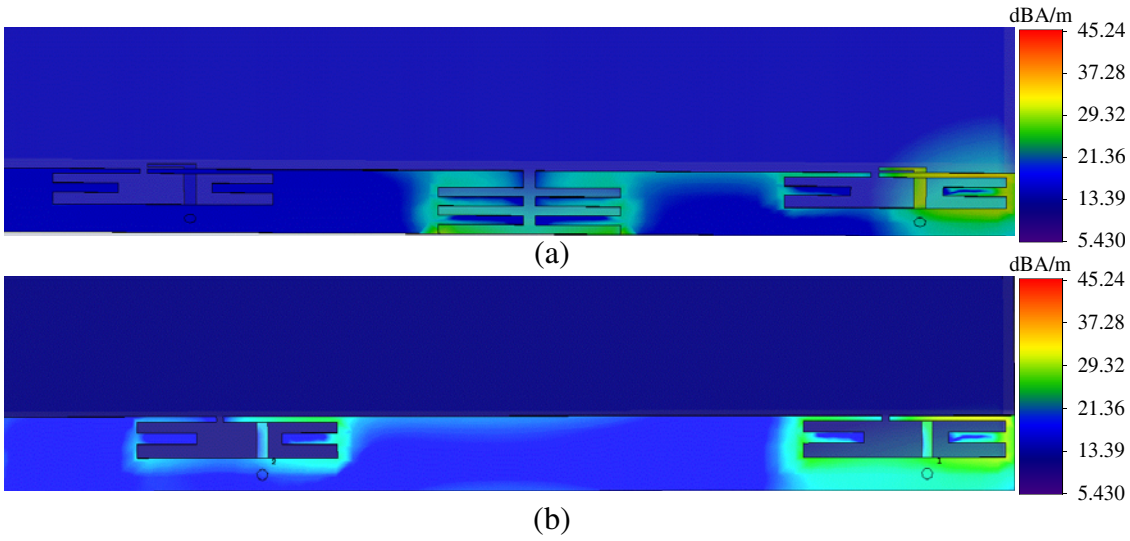

Figure 3. Current distribution on the antenna surface: (a) adding ladder-shaped DGS decoupling structure; and (b) without decoupling structure.

In order to reduce the interference between adjacent antennas in a compact space, a ladder-shaped DGS is designed. As shown in Figure 3, the current surrounds the defect to obtain the stopband characteristics and changes the antenna surface current distribution on the ground, thereby achieving good performance of diversity and multiplexing.

3. RESULT AND DISCUSSION

To verify the performance of the proposed antenna, a prototype is fabricated and measured, as shown in Figure 4. This MIMO antenna is simulated in CST Microwave Studio V18 and measured with Agilent E5072C vector network analyzer. The excitation port is connected to the test cable, while the irrelevant ports are terminated to 50-Ω broadband matched loads.

Figure 5 shows the simulated and measured S-parameters for Ants 1, 3, and 7. The simulated -10 dB impedance bandwidths are 280 MHz (3.34–3.62 GHz) and 460 MHz (4.67–5.13 GHz), which is sufficient to support the required Sub-6 GHz band. The simulated S_{13} with a DGS is below -20 dB, and S_{17} without decoupling structure is also below -17 dB. The measured reflection coefficient is lower than -10 dB in 3.41–3.58 GHz and 4.75–5.13 GHz bands, and the measured S_{13} and S_{17} are lower than

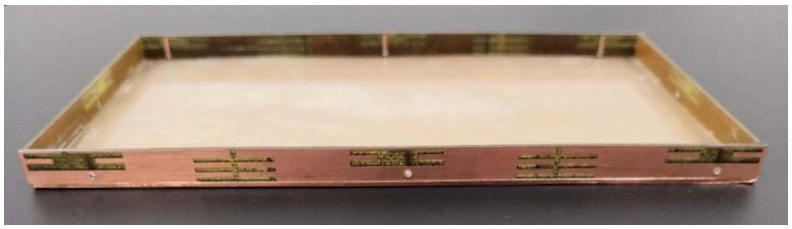

Figure 4. Photography of the fabricated prototype.

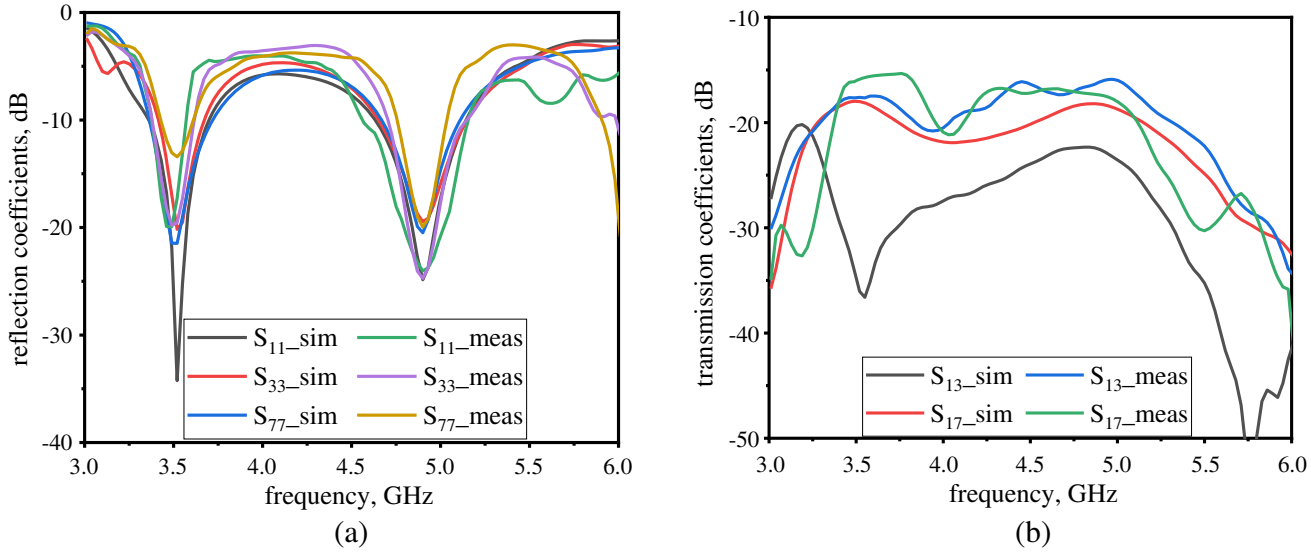

Figure 5. The S parameters for Ants 1, 3, 7: (a) reflection coefficients; and (b) transmission coefficients.

-15.2 dB. It can be observed that the results of the measured and simulated S-parameters are in good agreement.

Figure 6 shows the simulated and measured 2-D radiation patterns of Ants 1, 3, 7 in the E-plane (YZ) and H-plane (XZ). Due to the directional radiation characteristics of the slot antenna and the different positions of each antenna relative to the ground, the concentration of the antenna radiation pattern changes at certain angles. The difference between the simulation and measurement results may be the interference factors caused by the SMA connector and the measurement environment that are not considered in the simulation.

Since the DGS weakens the ground current while decoupling, the efficiency has a sinking point. As shown in Figure 7, the simulated results are always better than 70% within the operating frequency band. The measured antenna efficiencies are 50%–68% in the 3.5-GHz band and 55%–70% in the 4.9-GHz band. From the above measured results, it is confirmed that the proposed eight-element MIMO antenna can achieve good performances to meet the requirements for 5G terminal applications.

The diversity performance of MIMO antennas can be evaluated in terms of ECC. Assuming that the channel propagation model is uniformly distributed and the incident waves are isotropic in both directions of horizontal and vertical polarization, ECC can be calculated from the 3-D Complex E-field patterns of adjacent MIMO antenna elements as

$$\rho_e = \frac{\left| \iint\limits_{4\pi} \left[\vec{E}_1(\theta,\phi) \cdot \vec{E}_2(\theta,\phi) \right] d\Omega \right|^2}{\iint\limits_{4\pi} \left| \vec{E}_1(\theta,\phi) \right|^2 d\Omega \iint\limits_{4\pi} \left| \vec{E}_2(\theta,\phi) \right|^2 d\Omega} \tag{1}$$

where $\vec{E}_1(\theta,\phi)$ and $\vec{E}_2(\theta,\phi)$ are the electric field intensities of Ant1 and Ant2, respectively. As shown

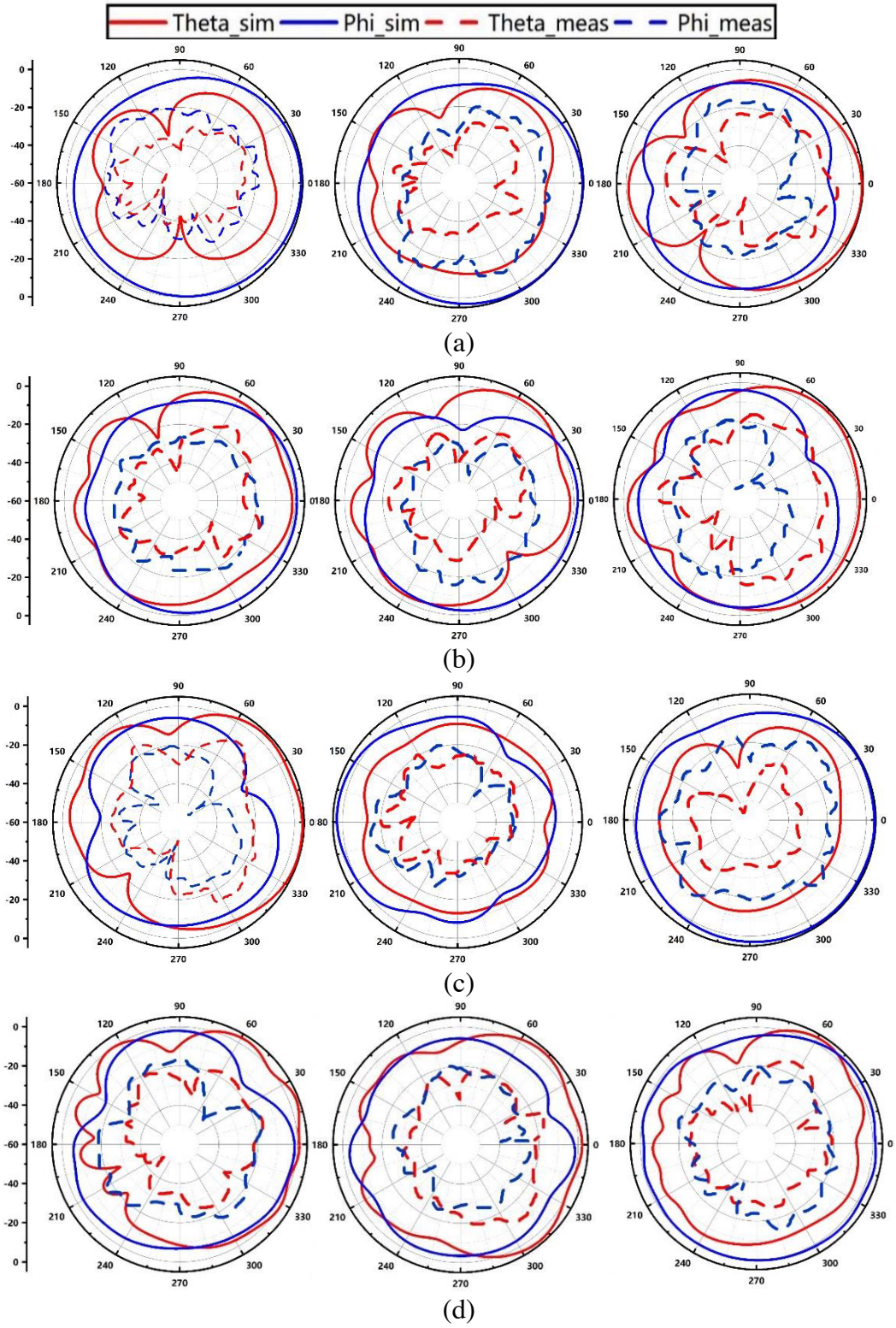

Figure 6. 2-D radiation patterns of the Ants 1, 3, and 7: (a) in the H-plane at 3.5 GHz; (b) in the H-plane at 4.9 GHz; (c) in the E-plane at 3.5 GHz; and (d) in the E-plane at 4.9 GHz.

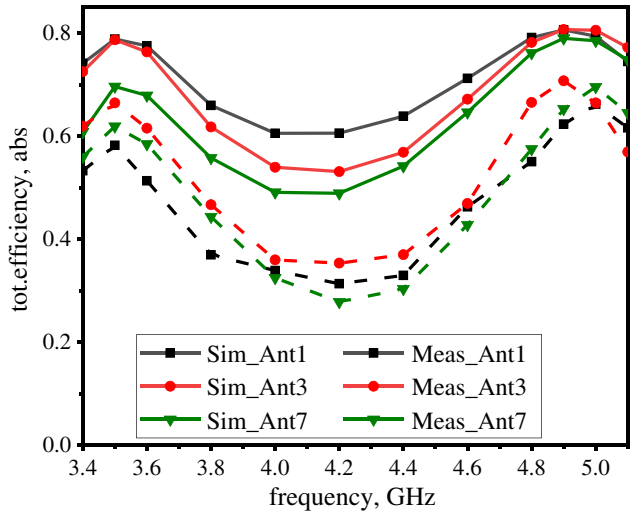

Figure 7. Radiation efficiencies of proposed Ants 1, 3 and 7.

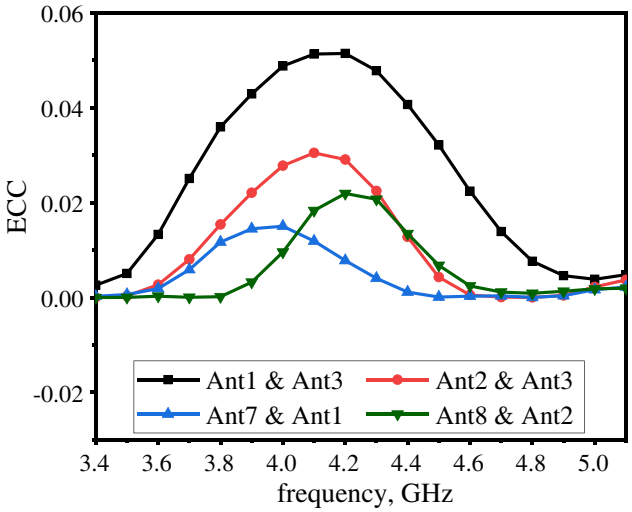

Figure 8. ECC of the proposed MIMO antenna.

Table 2. Comparison of the proposed MIMO antenna works.

Reference	Dimension of each element	$f_L - f_H$ (GHz)	Minimum isolation (dB)	Maximum efficiency (%)	ECC
[6]	$17 \times 4\,\text{mm}^2$	3.3–3.60 (−10 dB)	−10	76	0.15
[7]	$17 \times 6 \times 2.8\,\text{mm}^3$	2.52–2.68, 4.75–5.05 (−6 dB)	−10	83	0.20
[8]	$25 \times 15\,\text{mm}^2$	0.80–0.97, 1.80–2.87, 3.40–3.80, 5.15–5.85 (−10 dB)	−20	90	0.14
[9]	$20 \times 3\,\text{mm}^2$	3.40–3.60 (−10 dB)	−17.5	76	0.05
[12]	$24.8 \times 6.2\,\text{mm}^2$	3.40–3.60 (−10 dB)	−20	70	0.01
This work	$18.3 \times 2.5\,\text{mm}^2$	3.40–3.60, 4.70–5.10 (−10 dB)	−15	81	0.02

in Figure 8, the ECC is less than 0.02 in both operating bands and shows good spatial diversity characteristics.

Table 2 shows a comparison of this antenna with some other MIMO antenna works. Compared with [6–9, 12], the proposed antenna occupies less space with good isolation, high efficiency, and low ECC. Moreover, the proposed antenna designed around the handset frame cannot be easily interfered by various bottom components and is applicable to the currently popular full-screen mobile terminal.

4. CONCLUSION

In this letter, an eight-element multiple-input-multiple-output antenna system which consists of H-shaped slot antennas operating in 3.4–3.6 GHz and 4.7–5.1 GHz is presented for 5G mobile terminals applications. The dual-band characteristic is achieved by cutting a rectangular open end in the upper portion of the H-shaped slot. Moreover, the isolation among adjacent antennas is improved by etching the ladder-shaped DGS. The maximum efficiency in the operating frequency band is 81%, and the ECC is lower than 0.02. The simulated and measured results show that the antenna can generate good radiation diversity characteristics and satisfy the requirements of 5G communications.

REFERENCES

1. Huang, C., Y.-C. Jiao, and Z.-B. Weng, "Novel compact CRLH-TL-based tri-band MIMO antenna element for the 5G mobile handsets," *Microwave and Optical Technology Letters*, Vol. 60, No. 10, 2559–2564, Oct. 2018.
2. Das, G., A. Sharma, R. K. Gangwar, and M. S. Sharawi, "Compact back-to-back DRA-based four-port MIMO antenna system with bi-directional diversity," *Electronics Letters*, Vol. 54, No. 14, 884–886, 2018.
3. Wu, W., R. Zhi, Y. Chen, H. Li, Y. Tan, and G. Liu, "A compact multiband MIMO antenna for IEEE 802.11 a/b/g/n applications," *Progress In Electromagnetics Research Letters*, Vol. 84, 59–65, 2019.
4. Li, D.-H., F.-S. Zhang, L.-X. Cao, and Y. Zhao, "A compact dual band-rejected MIMO Vivaldi antenna for UWB wireless applications," *Progress In Electromagnetics Research Letters*, Vol. 86, 97–105, 2019.
5. Das, G., N. K. Sahu, A. Sharma, R. K. Gangwar, and M. S. Sharawi, "Dielectric resonator-based four-element eight-port MIMO antenna with multi-directional pattern diversity," *IET Microwaves, Antennas & Propagation*, Vol. 13, No. 1, 16–22, 2019.
6. Deng, J.-Y., J. Yao, D.-Q. Sun, and L.-X. Guo, "Ten-element MIMO antenna for 5G terminals," *Microwave and Optical Technology Letters*, Vol. 60, No. 12, 3045–3049, Dec. 2018.
7. Liu, D. Q., M. Zhang, H. J. Luo, H. L. Wen, and J. Wang, "Dual-band platform-free PIFA for 5G MIMO application of mobile devices," *IEEE Transactions on Antennas and Propagation*, Vol. 66, No. 11, 6328–6333, 2018.
8. Subbaraj, S., et al., "Performance enhancement and signal integrity analysis of multiband MIMO antenna for handheld electronic devices," *IET Microwaves, Antennas & Propagation*, Vol. 13, No. 5, 631–641, 2019.
9. Li, Y., C. Sim, Y. Luo, and G. Yang, "High-isolation 3.5-GHz 8-antenna MIMO array using balanced open slot antenna element for 5G smartphones," *IEEE Transactions on Antennas and Propagation*, Vol. 67, No. 6, 3820–3830, 2019.
10. Abdelrahim Ahmed, W. and Q. Feng, "A compact wideband slot antenna for universal UHF RFID reader," *Progress In Electromagnetics Research Letters*, Vol. 73, 137–144, 2018.
11. Saxena, S., B. K. Kanaujia, S. Dwari, S. Kumar, and R. Tiwari, "MIMO antenna with built-in circular shaped isolator for sub-6 GHz 5G applications," *Electronics Letters*, Vol. 54, No. 8, 478–480, 2018.
12. Zhao, A. and Z. Ren, "Size reduction of self-isolated MIMO antenna system for 5G mobile phone applications," *IEEE Antennas and Wireless Propagation Letters*, Vol. 18, No. 1, 152–156, 2019.